PHYSICAL REVIEW D **81,** 063515 (2010)

Bayesian analysis of the backreaction models

Aleksandra Kurek
Astronomical Observatory, Jagiellonian University, Orla 171, 30-244 Kraków, Poland[*]

Krzysztof Bolejko
Department of Mathematics and Applied Mathematics, University of Cape Town, Rondebosch 7701, South Africa and Nicolaus Copernicus Astronomical Center, Bartycka 18, 00-716 Warsaw, Poland[†]

Marek Szydłowski
Mark Kac Complex Systems Research Centre, Jagiellonian University, Reymonta 4, 30-059 Kraków, Poland and Dipartimento di Fisica Nucleare e Teorica, Università degli studi di Pavia, via A. Bassi 6, I-27100 Pavia, Italy[‡]
(Received 22 December 2008; revised manuscript received 18 November 2009; published 12 March 2010)

We present a Bayesian analysis of four different types of backreaction models, which are based on the Buchert equations. In this approach, one considers a solution to the Einstein equations for a general matter distribution and then an average of various observable quantities is taken. Such an approach became of considerable interest when it was shown that it could lead to agreement with observations without resorting to dark energy. In this paper we compare the ΛCDM model and the backreaction models with type Ia supernovae, baryon acoustic oscillations, and cosmic microwave background data, and find that the former is favored. However, the tested models were based on some particular assumptions about the relation between the average spatial curvature and the backreaction, as well as the relation between the curvature and curvature index. In this paper we modified the latter assumption, leaving the former unchanged. We find that, by varying the relation between the curvature and curvature index, we can obtain a better fit. Therefore, some further work is still needed—in particular, the relation between the backreaction and the curvature should be revisited in order to fully determine the feasibility of the backreaction models to mimic dark energy.

DOI: 10.1103/PhysRevD.81.063515 PACS numbers: 98.80.−k, 95.36.+x

I. INTRODUCTION

The Universe, as observed, is very inhomogenous on almost all scales. However, in a standard approach to cosmology, it is assumed that the Universe can be described by the homogeneous and isotropic Friedmann-Lemaître-Robertson-Walker (FLRW) models. The FLRW models provide a remarkably precise description of cosmological observations, but to achieve this we need to pay a price—in order to obtain concordance with observations it must be assumed that the Universe is filled with an unknown substance called dark energy. However, this substance has never been observed directly and, since it has very unusual properties, some have begun to ask whether dark energy is real or if it is the description of the Universe which, requires the existence of such an exotic entity, that is invalid.

While it is possible that our Universe is filled with dark energy, many alternatives have been proposed: braneworld cosmologies (see [1] for a review), $f(R)$ cosmology (see [2] for a review), application of inhomogeneous cosmological models (for a review see [3]) and others. One of the recently proposed approaches is based on an averaging framework. Such an approach is motivated by the fact that the Einstein equations are nonlinear, which means that the solution of the Einstein equations for a homogeneous matter distribution is different from the averaged solution to the Einstein equations for a general matter distribution. In other words, the evolution of the homogeneous model might be slightly different from the evolution of an inhomogeneous Universe, even though inhomogeneities in the Universe, when averaged over a sufficiently large scale, might tend to be zero. The difference between the evolutions of homogeneous and inhomogeneous models of the Universe is known as the backreaction effect. In this approach, one considers a solution to the Einstein equations for a general matter distribution and then an average of various observable quantities is taken. Under certain assumptions such an attempt leads to the Buchert equations [4]. The Buchert equations are very similar to the Friedmann equations, except for the backreaction term, which is in general nonvanishing if inhomogeneities are present. For a review on the backreaction effect and the Buchert averaging schemem the reader is referred to [5–7]. Based on this scheme, Larena *et al.* have recently proposed a model [8] in which the metric of the Universe at a given instant looks like the FLRW metric, but the evolution of the scale factor is governed by the Buchert equations. In this

[*]alex@oa.uj.edu.pl
[†]bolejko@camk.edu.pl
[‡]uoszydlo@cyf-kr.edu.pl

paper we aim to perform the Bayesian analysis of the cosmological observations within the models proposed in [8].

II. BACKREACTION MODELS

If the averaging procedure is applied to the Einstein equations then for irrotational, pressureless matter and 3 + 1 Arnowitt-Deser-Misner space-time foliation with a constant lapse and a vanishing shift vector, the following equations are obtained [4]:

$$3\frac{\ddot{a}}{a} = -4\pi G\langle\rho\rangle + \mathcal{Q}, \tag{1}$$

$$3\frac{\dot{a}^2}{a^2} = 8\pi G\langle\rho\rangle - \frac{1}{2}\langle\mathcal{R}\rangle - \frac{1}{2}\mathcal{Q}, \tag{2}$$

$$\mathcal{Q} \equiv \frac{2}{3}(\langle\Theta^2\rangle - \langle\Theta\rangle^2) - 2\langle\sigma^2\rangle, \tag{3}$$

where a dot (˙) denotes ∂_t, $\langle\mathcal{R}\rangle$ is an average of the spacial Ricci scalar ${}^{(3)}\mathcal{R}$, Θ is the scalar of expansion, σ is the shear scalar, ρ is the matter density, and $\langle\rangle$ is the volume average over the hypersurface of constant time: $\langle A\rangle = (\int d^3x\sqrt{-h})^{-1}\int d^3x\sqrt{-h}A$. The scale factor a is defined as a cube root of the volume

$$a = \left(\frac{V}{V_0}\right)^{1/3}, \tag{4}$$

where V_0 is an initial volume.

Equation (1) is compatible with (2) if the following integrability condition holds:

$$\frac{1}{a^6}\partial_t(\mathcal{Q}a^6) + \frac{1}{a^2}\partial_t(\langle R\rangle a^2) = 0. \tag{5}$$

Similarly, as in the FLRW models, the following parameters can be introduced:

$$H \equiv \frac{\dot{a}}{a}, \qquad \Omega_m \equiv \frac{8\pi G}{3H^2}\langle\rho\rangle, \qquad \Omega_{\mathcal{R}} \equiv -\frac{\langle\mathcal{R}\rangle}{6H^2}, \qquad \Omega_{\mathcal{Q}} \equiv -\frac{\langle\mathcal{Q}\rangle}{6H^2}. \tag{6}$$

The Hamiltonian constraints can then be written as

$$\Omega_m + \Omega_{\mathcal{R}} + \Omega_{\mathcal{Q}} = 1. \tag{7}$$

Observe that $\Omega_{\mathcal{R}} + \Omega_{\mathcal{Q}}$ can act like Ω_Λ. Moreover, if the dispersion of the expansion is large then $\mathcal{Q}$ can be large and as seen from (3), one can get acceleration ($\ddot{a} > 0$) without the need for dark energy.

The template metric of the Universe—the metric which describes the averaged universe can be written as

$$ds^2 = dt^2 - \frac{a(t)^2}{1 - k(t)r^2}dr^2 - a(t)^2r^2(d\vartheta^2 + \sin^2\vartheta d\varphi^2). \tag{8}$$

A similar approach, i.e. to consider the template metric with a scale factor which evolves accordingly to the Buchert equations instead of the Friedmann equations, was first introduced by Paranjape and Singh [9], though in their model k was constant. The motivation for $k(t)$ comes from the fact that the averaged spatial curvature, if calculated at one instant, does not have to be the same as the averaged spatial curvature calculated at another instant. This is closely related to the fitting problem studied by Ellis and Stoeger [10]. In considering the fitting problem, it becomes apparent that a homogeneous model fitted to inhomogeneous data can evolve quite differently from the real Universe. Therefore, if inhomogeneous model is averaged at one instant its FLRW parameters may be different from the FLRW parameters obtained after averaging at another instant.

The Buchert equations do not form a closed system. To close these equations and thus to calculate the evolution of the scale factor one has to introduce some further assumptions [4]. One such assumption can be $\langle\mathcal{R}\rangle \sim \mathcal{Q}$ [8]. As seen from the integrability condition (5), this leads to

$$\langle\mathcal{R}\rangle = \langle\mathcal{R}\rangle_i a^n \quad \text{and} \quad \mathcal{Q} = -\frac{n+2}{n+6}\langle\mathcal{R}\rangle_i a^n, \tag{9}$$

where n is an arbitrary parameter. Now, the final step is to derive a relation between the average spacial curvature $\langle\mathcal{R}\rangle$ and the curvature index k. In analogy to the FLRW models, the following relation can be proposed [8]:

$$k = \frac{a^2\langle\mathcal{R}\rangle}{a_i^2|\langle\mathcal{R}\rangle_i|} \to k(z) = -\frac{(n+6)(1-\Omega_m)(1+z)^{-(n+2)}}{|(n+6)(1-\Omega_m)|}. \tag{10}$$

In Sec. III B 2 we will modify the above assumption and test models with different relations between k and $\langle\mathcal{R}\rangle$. Summarizing, the model considered in this paper is described by the metric (8), but the evolution of the scale factor is governed by the Buchert equations. Employing the assumptions (9) and (10) the evolution equations reduce to the following relation:

$$H = H_0\sqrt{\Omega_m(1+z)^3 + (1-\Omega_m)(1+z)^{-n}}. \tag{11}$$

This model is parametrized by two parameters: Ω_m and n. The distance, using (8), can then be calculated by solving

$$\frac{dr}{dz} = \sqrt{\frac{1-kr^2}{\Omega_m(1+z)^3 + (1-\Omega_m)(1+z)^{-n}}}. \tag{12}$$

Larena *et al.* [8] tested this model with a likelihood analysis using the supernova and cosmic microwave background (CMB) data. They found that this model is in good agreement with observations. In the next section we will perform the Bayesian analysis of this model using the SNIa data, baryon acoustic oscillations (BAO) and the observation of the CMB radiation.

III. BAYESIAN ANALYSIS

The model presented in the preceding section will be confronted with cosmological observations in the Bayesian framework using the COSMONEST code [11,12], which was adapted to our case. In the Bayes theory all that we know about the vector of parameters ($\bar{\theta}$) of a given model (M) is contained in the posterior probability density function (PDF), which is given by [26]

$$P(\bar{\theta}|D, M) = \frac{P(D|\bar{\theta}, M)P(\bar{\theta}|M)}{P(D|M)}, \tag{13}$$

where D denotes the set of data used in the analysis; $P(D|\bar{\theta}, M)$ is the likelihood function for a given model, which will henceforth be referred to as $L(\bar{\theta})$; $P(\bar{\theta}|M)$ is the prior PDF, which enables us to include our previous knowledge (i.e. without information coming from the data D) about the parameters under consideration; and the last quantity $P(D|M)$ is the normalization constant, called the evidence (or marginal likelihood), which is the most important quantity in the Bayesian framework of model comparison. The posterior PDF could be simply summarized in terms of a best-fit value, which could be the posterior PDF mode (the most probable value of $\bar{\theta}$) or the mean of the marginal posterior PDF of a given parameter (θ_i), obtained by integration (13) over the remaining parameters.

A. Parameters estimation

1. Supernova data

Firstly, we consider observations of type Ia supernova, which are taken from the Supernova Legacy Survey (SNLS) [15] and the Union Supernova Compilation [16]. After analytical marginalization over the H_0 parameter the likelihood function is of the following form:

$$L_{SN}(\Omega_m, n) \propto \exp\left[-\frac{1}{2}\left(\sum_{i=1}^{N}\frac{x_i^2}{\sigma_i^2} - \frac{(\sum_{i=1}^{N}\frac{x_i}{\sigma_i^2})^2}{\sum_{i=1}^{N}\frac{1}{\sigma_i^2}}\right)\right], \tag{14}$$

where N is the number of data points ($N = 115$ for the SNLS sample and $N = 307$ for the Union sample), σ_i is the observational error [17], $x_i = \mu_i^{\text{theor}} - \mu_i^{\text{obs}}$, with $\mu_i^{\text{obs}} = m_i - M$ (m_i is the apparent magnitude and M the absolute magnitude of SNIa), is the observed distance moduli [18], $\mu_i^{\text{theor}} = 5\log_{10}D_L + 25$, where $D_L = cr(1 + z)$ is the luminosity distance, and r is given by (12).

We assume flat prior PDFs for the model parameters over their entire assumed ranges. The allowed range of Ω_m is the same as the one used to constrain the ϕ function of Eq. (15) [19], i.e. $\Omega_m \in [0.2, 0.6]$. Finally, since we are interested in a wide range of models, we choose the parameter n to vary over a wide range $n \in [-4, 4]$.

The results are presented in Fig. 1. As seen, the higher Ω_m, the higher n must be taken in order to obtain a satisfactory fit. Also, the Union data set puts tighter constraints on the allowed range of the model parameters, although it prefers higher values of Ω_m and n.

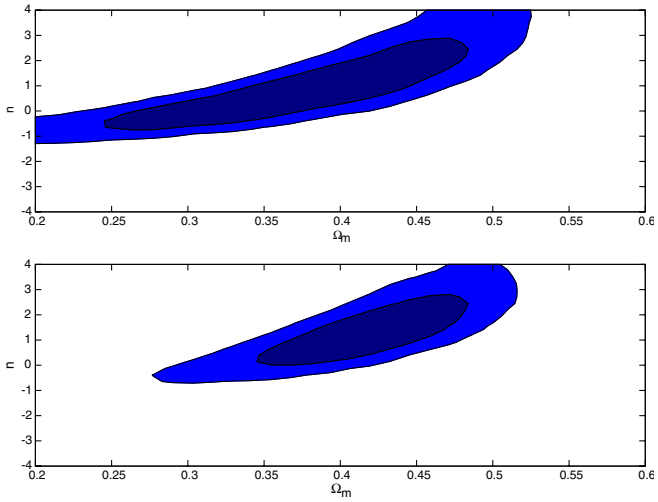

FIG. 1 (color online). Constraints from SN data (SNLS—upper panel, Union—lower panel). 68% and 95% contours are presented.

2. CMB data

The second set of cosmological observations comprises measurement of the CMB angular power spectrum. Here, we present the analysis of the CMB data which is restricted only to fitting the positions of the first two peaks and the first trough. Such analysis therefore ignores the shape of the CMB power spectrum. One, therefore. should keep in mind that the full CMB constraints are tighter [20].

If it is assumed that the early Universe (before and up to the last scattering instant) is well described by the FLRW model then the CMB power spectrum can be parametrized by [19]

$$l_m = l_a(m - \phi_m), \tag{15}$$

where l_1, l_2, and l_3 are the positions of the first, second, and third peaks, and

$$l_a = \pi\frac{r_*}{r_s}, \tag{16}$$

where r_* is the comoving distance to the last scattering surface and r_s is the size of the sound horizon at the last scattering instant. The function ϕ_m describes the phase shift of the m-th peak and is mainly sensitive to prerecombination physics. It depends on the baryon density ($\Omega_b h^2$), where $h = H_0/(100\ \text{Mpc km s}^{-1})$, on the ratio of the radiation to matter density at last scattering $[\rho_r(z_*)/\rho_m(z_*) = 0.042(\Omega_m h^2)^{-1}(z_*/10^3)]$, where z_* is the recombination redshift, on the spectral index (n_s), and on the density of the dark energy before recombination.

We fit the positions of the first and second peaks, and the first trough of the CMB power spectrum [21]. We assume that $n_s = 1$ and neglect the density of dark energy before recombination. $r_* = c/H_0 r(z_*)$, $r(z)$ is given by (12) and $r_s = c(2/3k_{\rm eq})\sqrt{6/R_{\rm eq}}\ln[(\sqrt{1+R_*}+\sqrt{R_*+R_{\rm eq}})/(1+\sqrt{R_{\rm eq}})]$, where $R_{\rm eq} = R/(1+z_{\rm eq})$, $R_* = R/(1+z_*)$, $k_{\rm eq} = H_0\sqrt{2\Omega_m z_{\rm eq}}$, $R = 31\,500\Omega_b h^2(T_{\rm CMB}/2.7K)^{-4}$ and $z_{\rm eq} = 2.5\times 10^4\Omega_m h^2(T_{\rm CMB}/2.7K)^{-4}$. We take $T_{\rm CMB} = 2.728$ and employ the fitting formulae for z_* as provided in Ref. [22].

We use the position of the peaks and trough locations in the CMB power spectrum coming from the WMAP3 measurements [21]. Those values were obtained in an almost model independent manner. The power spectra was fitted by the model composed of a Gaussian peak, parabolic trough and a second parabolic peak. Such model contains eight independent parameters, including peaks and though positions. Constraints were obtained using Markov chain Monte Carlo method. The values and uncertainties of these parameters are the maximum and the width of the posterior probability distribution function. Additionally, the uncertainties include calibration uncertainty and cosmic variance. The likelihood function could be therefore written in the following form:

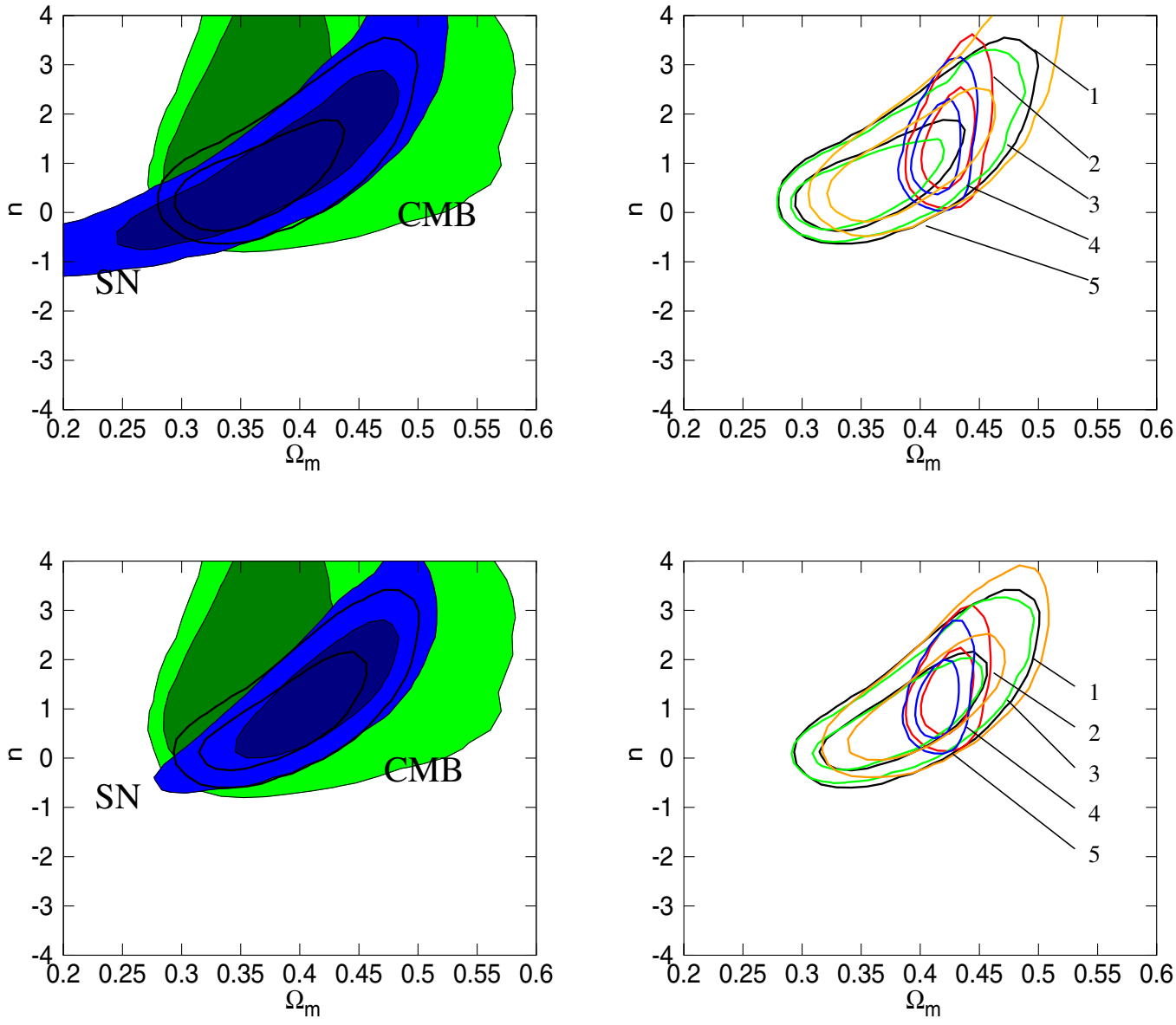

FIG. 2 (color online). Left panels: constraints from SN, CMB, and SN + CMB data (SNLS + CMB—upper panel, Union + CMB—lower panel). Right panels: comparison of constraints from SN + CMB data (SNLS + CMB—upper panel, Union + CMB—lower panel) with different prior assumptions on the parameters h and $\Omega_b h^2$: case 1, case 2, case 3, case 4, case 5.

$$L_{\mathrm{CMB}}(\Omega_m, n, \Omega_b h^2, h) \propto \exp\Big[-\frac{1}{2}\Big(\Big(\frac{l_1 - 220.8}{0.7}\Big)^2 + \Big(\frac{l_{3/2} - 412.4}{1.9}\Big)^2 + \Big(\frac{l_2 - 530.9}{3.8}\Big)^2\Big)\Big]. \quad (17)$$

We assume flat prior PDFs for the model parameters in the ranges (case 1): $\Omega_m \in [0.2, 0.6]$, $n \in [-4, 4]$, $h \in [0.64, 0.80]$ (using information from Hubble Space Telescope [23]), $\Omega_b h^2 \in [0.0203, 0.0223]$ (using information from big bang nucleosynthesis (BBN) [24]).

The 68% and 95% contours of the posterior PDFs (after marginalization over h and $\Omega_b h^2$), obtained in the analysis with the CMB data as well as in the analysis with the joint data set (SNIa + CMB) (here, the likelihood function has the following form: $L = L_{\mathrm{SN}} L_{\mathrm{CMB}}$) are presented in Fig. 2 (left panels). As seen both data sets prefer $n > -1$. However, unlike SNIa, CMB data prefers lower values of Ω_m, but still the best fits are consistent with each other.

The marginal posterior PDFs are presented in Figs. 3 and 4 (case 1). As seen, preferred values of Ω_m are higher than inferred within the standard cosmological model. The means together with the 68% Bayesian confidence intervals (credible intervals) and the posterior modes are pre-

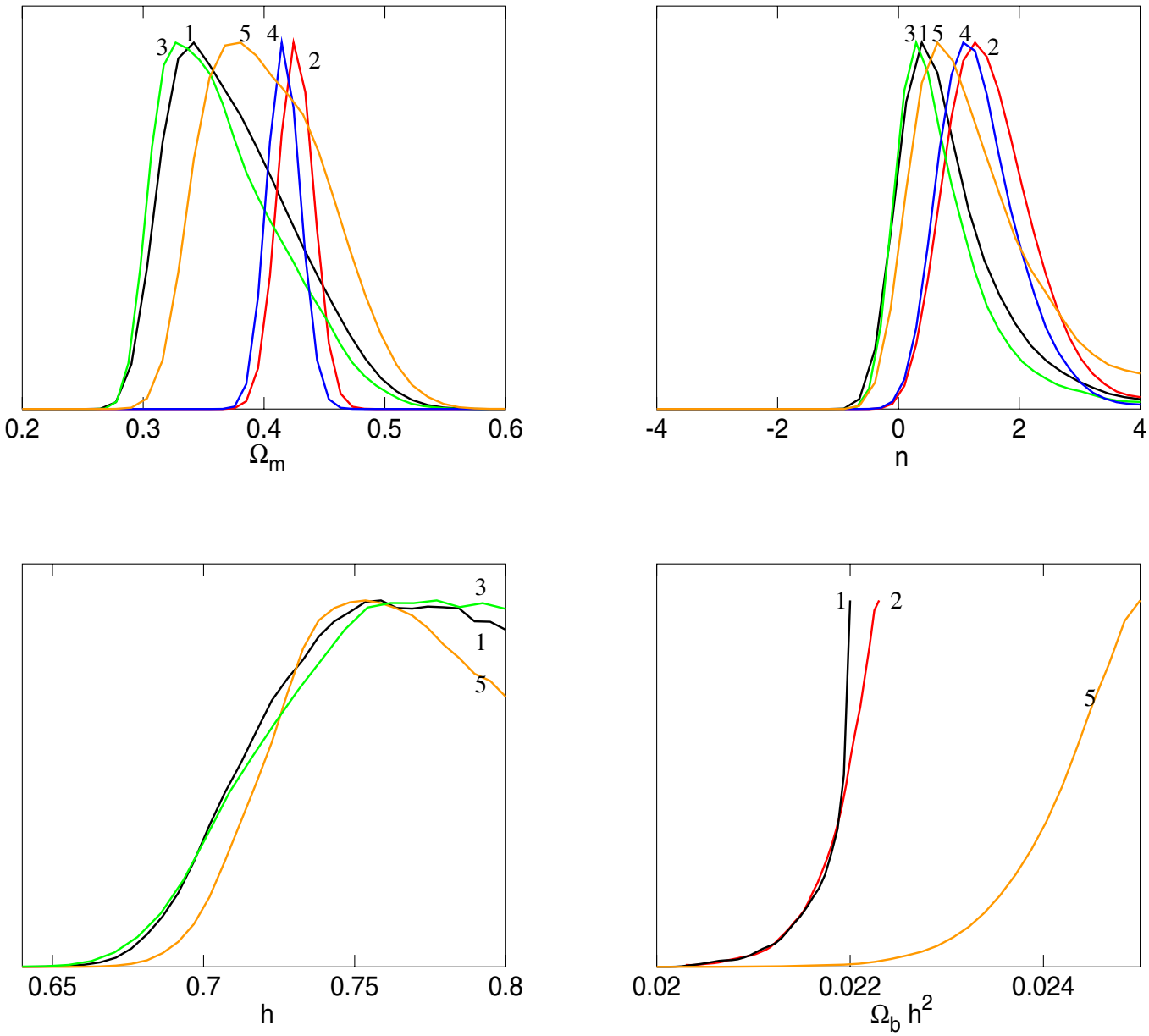

FIG. 3 (color online). Marginal posterior PDFs for model parameters (SNLS + CMB) with different prior assumption on h and $\Omega_b h^2$ parameters: case 1, case 2, case 3, case 4, case 5.

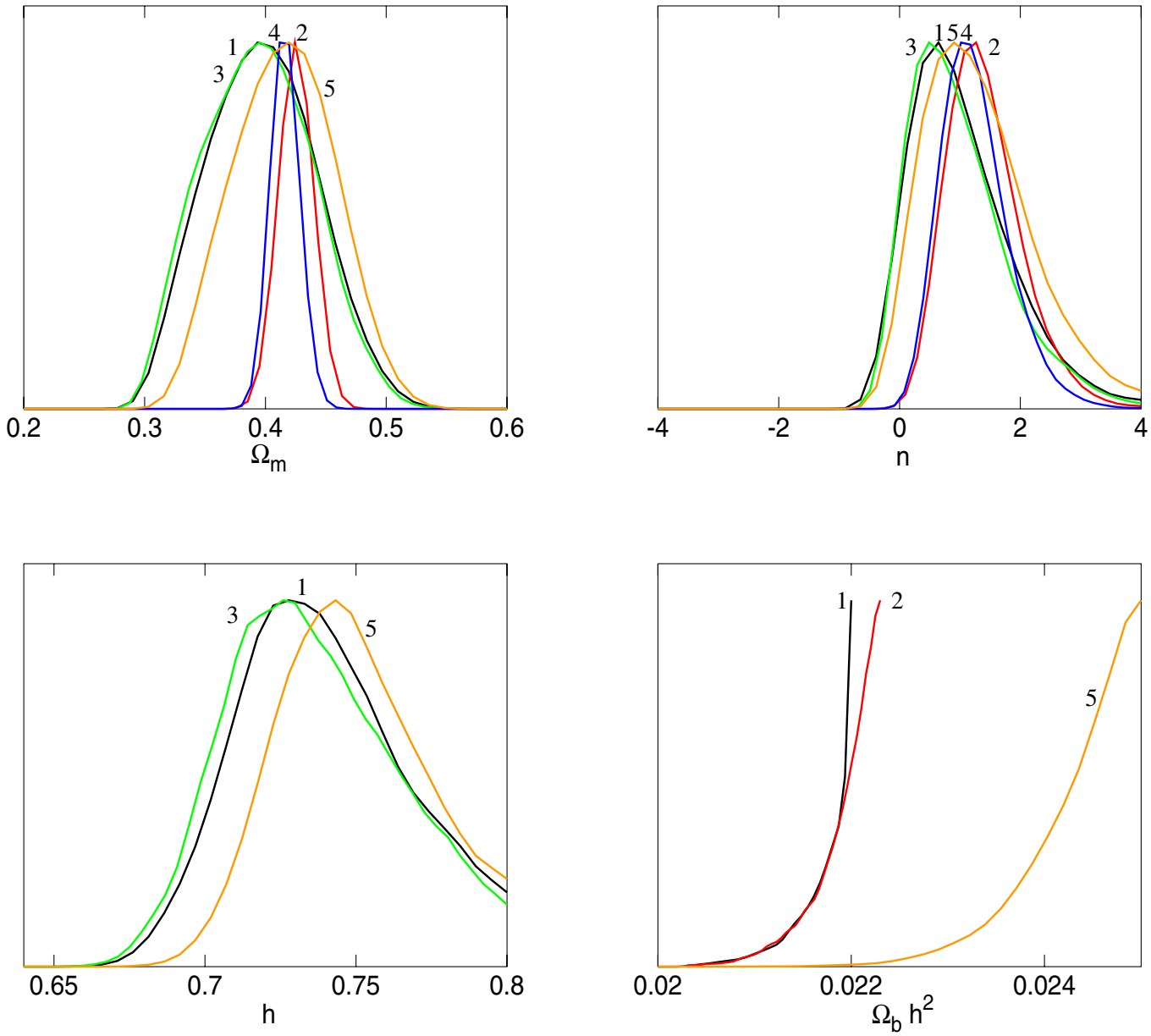

FIG. 4 (color online). Marginal posterior PDFs for model parameters (Union + CMB) with different prior assumption on h and $\Omega_b h^2$ parameters: case 1, case 2, case 3, case 4, case 5.

sented in Tables I and II for SNLS + CMB and Union + CMB, respectively. An interesting observation is that the mean of n is around 1. When $n = 0$, the $H(z)$ does not depend on the spatial curvature. Hence, if only expansion history is considered, in such a case the backreaction effect behaves as the cosmological constant. When $n = 2$, the $H(z)$ depends on the spatial curvature as in FLRW models.

It is interesting to see how constraints on the Ω_m and n are changed after changing the prior information on the h and $\Omega_b h^2$ parameters. We consider four different situations: case 2—we fix the value of the Hubble parameter to the best-fit value obtained in [23], i.e. $h = 0.72$; case 3—we fix the value of $\Omega_b h^2$ to the best-fit value obtained in [24], i.e. $\Omega_b h^2 = 0.0213$; case 4—we fix the values of both parameters ($h = 0.72$ and $\Omega_b h^2 = 0.0213$). We observe that, CMB and SNIa data considered together prefer larger values of $\Omega_b h^2$ than expected from BBN constraints. Because of this we additionally check how the results are changed after allowing the $\Omega_b h^2$ parameter to take larger values, i.e. expand the prior range to $(\Omega_b h^2)^* \in [0.020, 0.025]$ (case 5). Constraints from SNIa and CMB data on the Ω_m and n parameters for the cases described above are shown in the right panel of Fig. 2. The largest changes occur when the Hubble parameter is fixed (cases 2 and 4). The values of Ω_m and n are shifted to larger values and the constraints become tighter (especially for

TABLE I. Means of the marginal posterior PDFs for the model parameters, together with the 68% credible intervals for the SNIa + CMB and SNIa + CMB + BAO data sets. The corresponding values for the posterior modes are presented in brackets.

	SNLS + CMB	SNLS + CMB + BAO
Ω_m	$0.37^{+0.06}_{-0.04}(0.32)$	$0.42^{+0.04}_{-0.05}(0.40)$
n	$0.87^{+0.78}_{-0.71}(0.00)$	$1.59^{+0.91}_{-0.85}(1.48)$
h	$0.75^{+0.03}_{-0.03}(0.79)$	$0.73^{+0.02}_{-0.03}(0.73)$
$\Omega_b h^2$	$0.0219^{+0.0003}_{-0.0003}(0.0223)$	$0.0219^{+0.0003}_{-0.0003}(0.0223)$
Ω_m	$0.43^{+0.01}_{-0.02}(0.43)$	$0.43^{+0.01}_{-0.02}(0.43)$
n	$1.55^{+0.69}_{-0.69}(1.48)$	$1.70^{+0.71}_{-0.70}(1.68)$
h	0.72	0.72
$\Omega_b h^2$	$0.0219^{+0.0003}_{-0.0003}(0.0222)$	$0.0219^{+0.0003}_{-0.0003}(0.0223)$
Ω_m	$0.37^{+0.05}_{-0.05}(0.31)$	$0.41^{+0.04}_{-0.05}(0.40)$
n	$0.76^{+0.67}_{-0.66}(-0.05)$	$1.46^{+0.83}_{-0.79}(1.17)$
h	$0.75^{+0.03}_{-0.03}(0.80)$	$0.72^{+0.03}_{-0.02}(0.73)$
$\Omega_b h^2$	0.0213	0.0213
Ω_m	$0.42^{+0.01}_{-0.01}(0.41)$	$0.42^{+0.01}_{-0.01}(0.41)$
n	$1.36^{+0.64}_{-0.61}(1.15)$	$1.53^{+0.62}_{-0.63}(1.29)$
h	0.72	0.72
$\Omega_b h^2$	0.0213	0.0213
Ω_m	$0.40^{+0.05}_{-0.05}(0.34)$	$0.44^{+0.04}_{-0.04}(0.45)$
n	$1.27^{+0.97}_{-0.89}(0.27)$	$2.01^{+1.10}_{-0.88}(2.00)$
h	$0.75^{+0.03}_{-0.02}(0.79)$	$0.73^{+0.02}_{-0.02}(0.73)$
$(\Omega_b h^2)^*$	$0.0243^{+0.0005}_{-0.0005}(0.0248)$	$0.0243^{+0.0005}_{-0.0006}(0.0245)$

TABLE II. Means of the marginal posterior PDFs for the model parameters together with the 68% credible intervals for the SNIa + CMB and SNIa + CMB + BAO data sets. The corresponding values for the posterior modes are presented in brackets.

	Union + CMB	Union + CMB + BAO
Ω_m	$0.40^{+0.04}_{-0.05}(0.36)$	$0.43^{+0.03}_{-0.04}(0.42)$
n	$1.02^{+0.79}_{-0.77}(0.35)$	$1.60^{+0.80}_{-0.76}(1.14)$
h	$0.74^{+0.03}_{-0.03}(0.76)$	$0.72^{+0.02}_{-0.02}(0.72)$
$\Omega_b h^2$	$0.0219^{+0.0003}_{-0.0003}(0.0223)$	$0.0219^{+0.0003}_{-0.0003}(0.0223)$
Ω_m	$0.42^{+0.02}_{-0.01}(0.43)$	$0.43^{+0.01}_{-0.02}(0.42)$
n	$1.41^{+0.58}_{-0.58}(1.51)$	$1.57^{+0.61}_{-0.60}(1.34)$
h	0.72	0.72
$\Omega_b h^2$	$0.0219^{+0.0003}_{-0.0003}(0.0223)$	$0.0219^{+0.0003}_{-0.0003}(0.0223)$
Ω_m	$0.39^{+0.05}_{-0.04}(0.38)$	$0.42^{+0.04}_{-0.03}(0.42)$
n	$0.97^{+0.76}_{-0.75}(0.48)$	$1.48^{+0.73}_{-0.74}(1.40)$
h	$0.73^{+0.03}_{-0.02}(0.74)$	$0.72^{+0.02}_{-0.02}(0.72)$
$\Omega_b h^2$	0.0213	0.0213
Ω_m	$0.42^{+0.01}_{-0.01}(0.41)$	$0.42^{+0.01}_{-0.01}(0.41)$
n	$1.25^{+0.53}_{-0.52}(1.07)$	$1.39^{+0.53}_{-0.53}(1.23)$
h	0.72	0.72
$\Omega_b h^2$	0.0213	0.0213
Ω_m	$0.41^{+0.05}_{-0.04}(0.39)$	$0.44^{+0.03}_{-0.03}(0.44)$
n	$1.30^{+0.85}_{-0.84}(0.83)$	$1.92^{+0.84}_{-0.81}(1.94)$
h	$0.75^{+0.02}_{-0.03}(0.77)$	$0.73^{+0.02}_{-0.02}(0.74)$
$(\Omega_b h^2)^*$	$0.0244^{+0.0005}_{-0.0006}(0.0249)$	$0.0243^{+0.0005}_{-0.0005}(0.0249)$

the matter density). On the other hand, fixing the value of $\Omega_b h^2$ does not give substantial changes in the constraints (cases 3 and 4). We can see that expanding the allowed range shifts the best-fit values of Ω_m and n upwards but does not improve the constraints (case 5). This can also be seen on the marginal posterior PDF plots. One can additionally conclude that fixing the value of $\Omega_b h^2$ does not have any influence on the marginal posterior PDF for h (case 3), but expanding the allowed range of $\Omega_b h^2$ changes it slightly (case 5). Fixing the value of h does not influence the posterior PDF of $\Omega_b h^2$ (case 2). SNIa and CMB data considered together prefer larger values of $\Omega_b h^2$, even when an extension of the allowed range is considered (case 5). As one can see, changes in the constraints on the Ω_m and n parameters are more prominent when the SNLS data set is considered. The means together with the 68% Bayesian confidence intervals (credible intervals), and the posterior modes are presented in Tables I and II for SNLS + CMB and Union + CMB, respectively.

3. BAO data

In addition to the geometric measurements described above, we study constraints obtained from the measured dilation scale of the BAO in the redshift space power-spectrum of 46 748 luminous red galaxies from the Sloan Digital Sky Survey. The dilation scale is defined as

$$D_V = \left[D_A^2 \frac{cz}{H(z)} \right]^{1/3}, \tag{18}$$

where D_A is the comoving angular diameter distance and $H(z)$ is the Hubble parameter as a function of redshift. The measured value of the dilation scale at $z = 0.35$ is 1370 ± 64 Mpc. It should be noted that the value of 1370 ± 64 Mpc was obtained within the framework of linear perturbations imposed on the homogeneous FLRW background. Instead, such an analysis should be carried out within the framework of the model considered in this paper. Otherwise, we should be aware of possible systematical errors. When the geometry of the space-time is not FLRW the possible sources of errors are (1) the sound horizon can be distorted and can be of a different size in parallel and perpendicular directions; (2) the expansion rate can be different with respect to parallel and perpendicular directions; (3) the redshift distortions, if analyzed within the inhomogeneous model, might lead to estimates different from those received within the standard approach; (4) another source of error comes from the fact that in their analysis Eisenstein *et al.* converted the redshifts of luminous red galaxies to distances assuming the ΛCDM model. Despite these uncertainties we proceed with the analysis to see how the BAO data can possibly constrain the data. As seen from Fig. 5, the measurements of the dilation scale at $z = 0.35$ do not put tight constraints on the parameters of

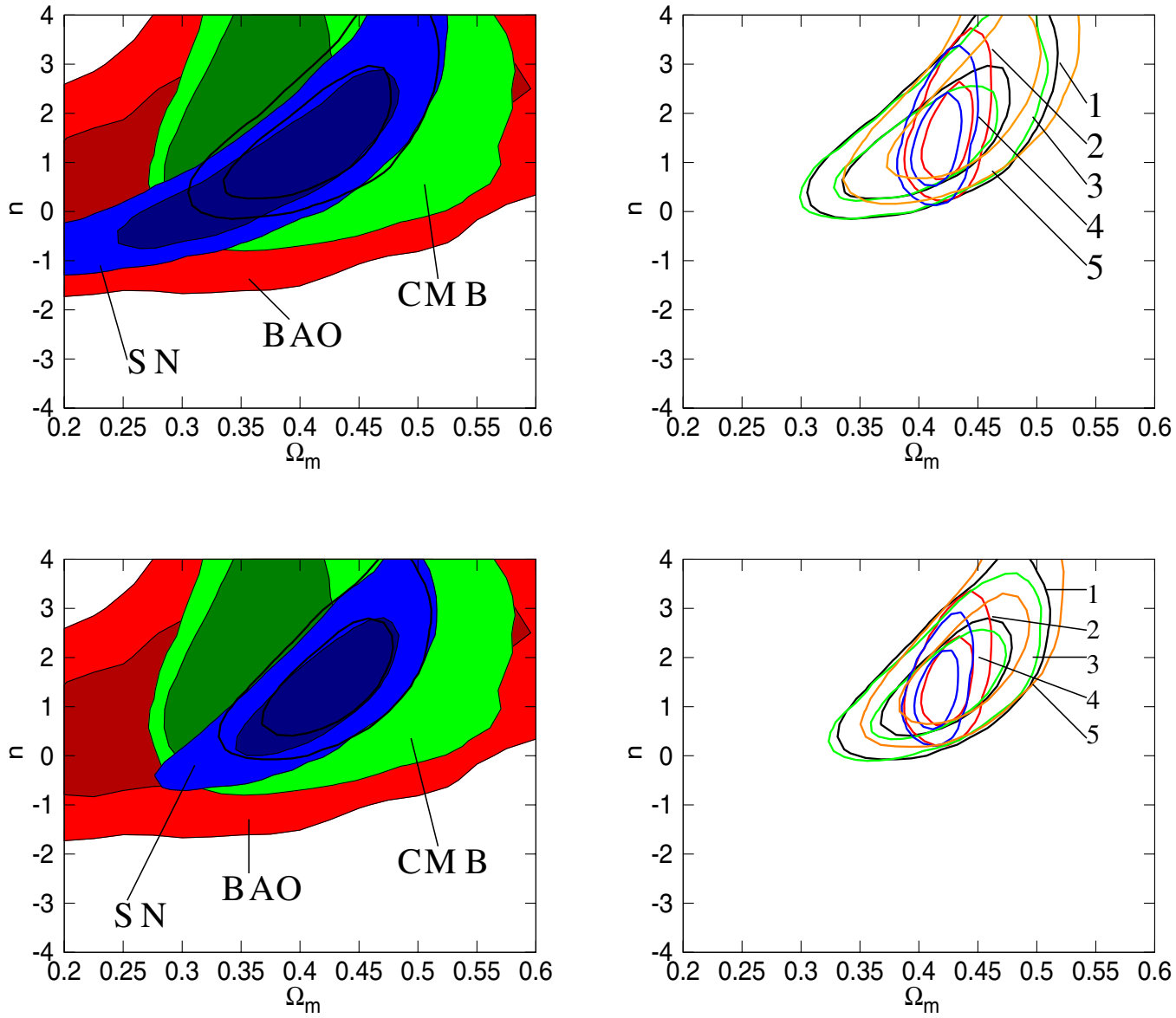

FIG. 5 (color online). Left panels: constraints from SNIa, CMB , BAO, and SNIa + CMB + BAO data sets (SNLS + CMB + BAO—upper panel, Union + CMB + BAO—lower panel). Right panels: comparison of constrains from SN + CMB + BAO data (SNLS + CMB + BAO—upper panel, Union + CMB + BAO—lower panel) with different prior assumption on h and $\Omega_b h^2$ parameters: case 1, case 2, case 3, case 4, case 5.

the model. At higher redshifts the constraints will be tighter, and thus an analysis of the BAO within the backreaction model will be required when future observational data is available. The likelihood function for the BAO has the following form:

$$L_{\mathrm{BAO}}(\Omega_m, n, h) \propto \exp\left[-\frac{(D_V^{\mathrm{theor}} - D_V^{\mathrm{obs}})^2}{2\sigma_{\mathrm{BAO}}^2}\right]. \quad (19)$$

We assume flat prior PDFs for the parameters within the ranges described above for case 1. The 68% and 95% contours of the posterior PDF (marginalized over h and $\Omega_b h^2$) for the joint constraints from the supernovae, CMB and BAO data (with the likelihood function of the following form: $L = L_{\mathrm{SN}} L_{\mathrm{CMB}} L_{\mathrm{BAO}}$) are presented in Fig. 5 (case 1).

The marginal posterior PDFs are presented in Figs. 6 and 7 (case 1). In comparison with the preceding section, the PDFs are similar except for n, which is now shifted to higher values. The means of the marginal posterior PDFs together with the 68% credible intervals are presented in Tables I and II for SNLS + CMB + BAO and Union + CMB + BAO, respectively. For example, n based on Union + CMB + BAO is now $1.60^{+0.80}_{-0.76}$ in comparison to $1.02^{+0.79}_{-0.77}$ inferred only from Union + CMB. We will come back to the relation between the curvature and backreaction effects in Sec. III B 2. We also check how the

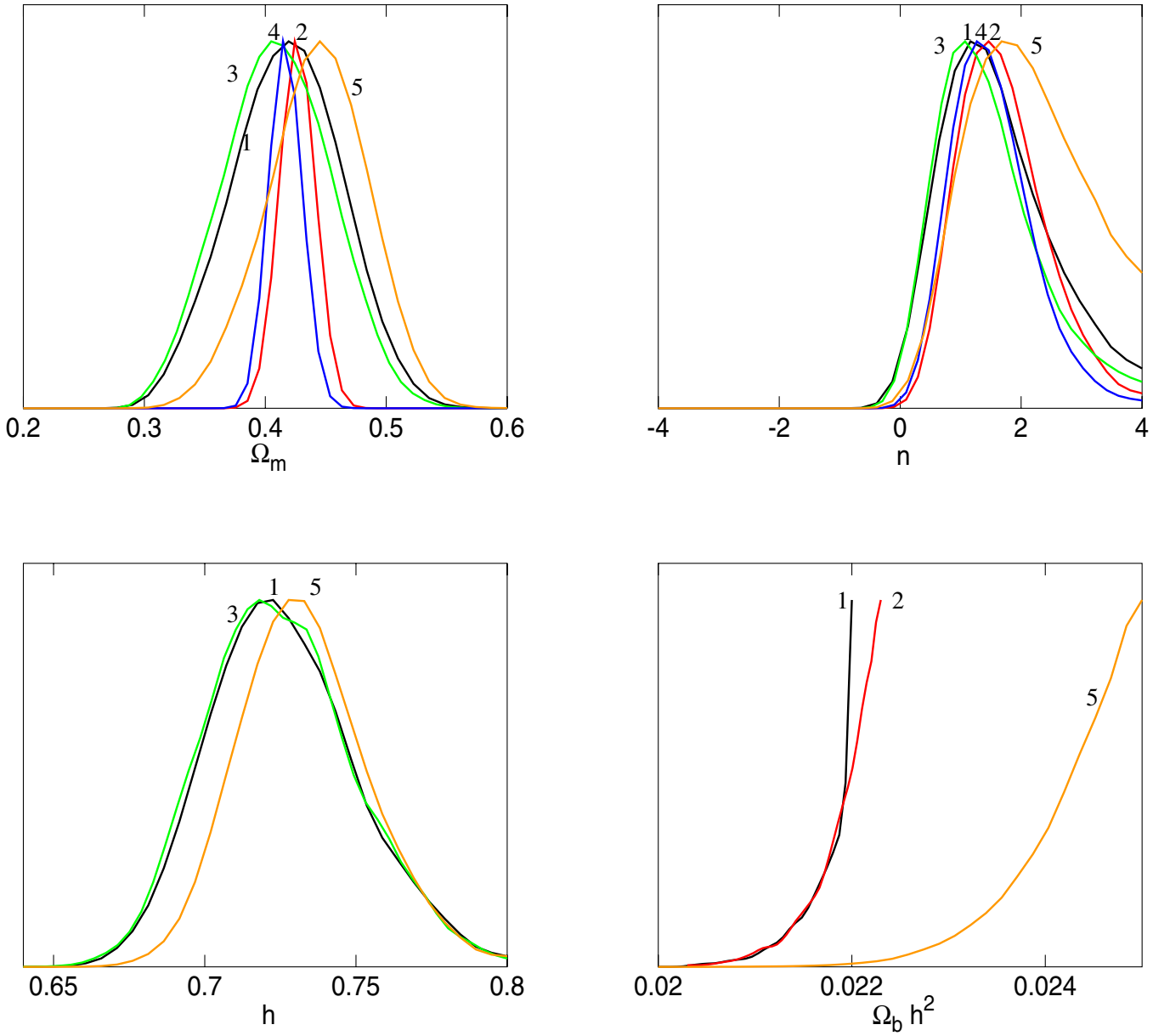

FIG. 6 (color online). Marginal posterior PDFs for model parameters (SNLS + CMB + BAO) with different prior assumptions on the parameters h and $\Omega_b h^2$: case 1, case 2, case 3, case 4, case 5.

results are sensitive to changes in the prior information for the h and $\Omega_b h^2$ parameters. We consider all cases described above. Observe that changes are most prominent when the value of h is fixed. The contours become narrower (cases 2 and 4 on the right panels of Fig. 5), which is due to tighter constraints on the Ω_m parameter. The values of Ω_m and n do not change significantly. When we expand the allowed prior range for the parameter $\Omega_b h^2$, the values of Ω_m and n are slightly shifted upwards, and the constraints on n become weaker (see also the posterior PDFs presented in Fig. 6 and 7). Constraints on h are also changed in this case: its value is shifted upwards.

An interesting point is that the PDF of $\Omega_b h^2$ increases with $\Omega_b h^2$ and does not seem to decrease in the considered range. This implies that the maximum of the PDF is out of the range and might suggest a tension between SNIa + CMB, SNIa + CMB + BAO and BBN constraints on $\Omega_b h^2$.

B. Models comparison

1. ΛCDM *vs the backreaction model*

In this section we present the comparison between the model considered above (which will be referred to as model 1) and the ΛCDM model (which will be referred

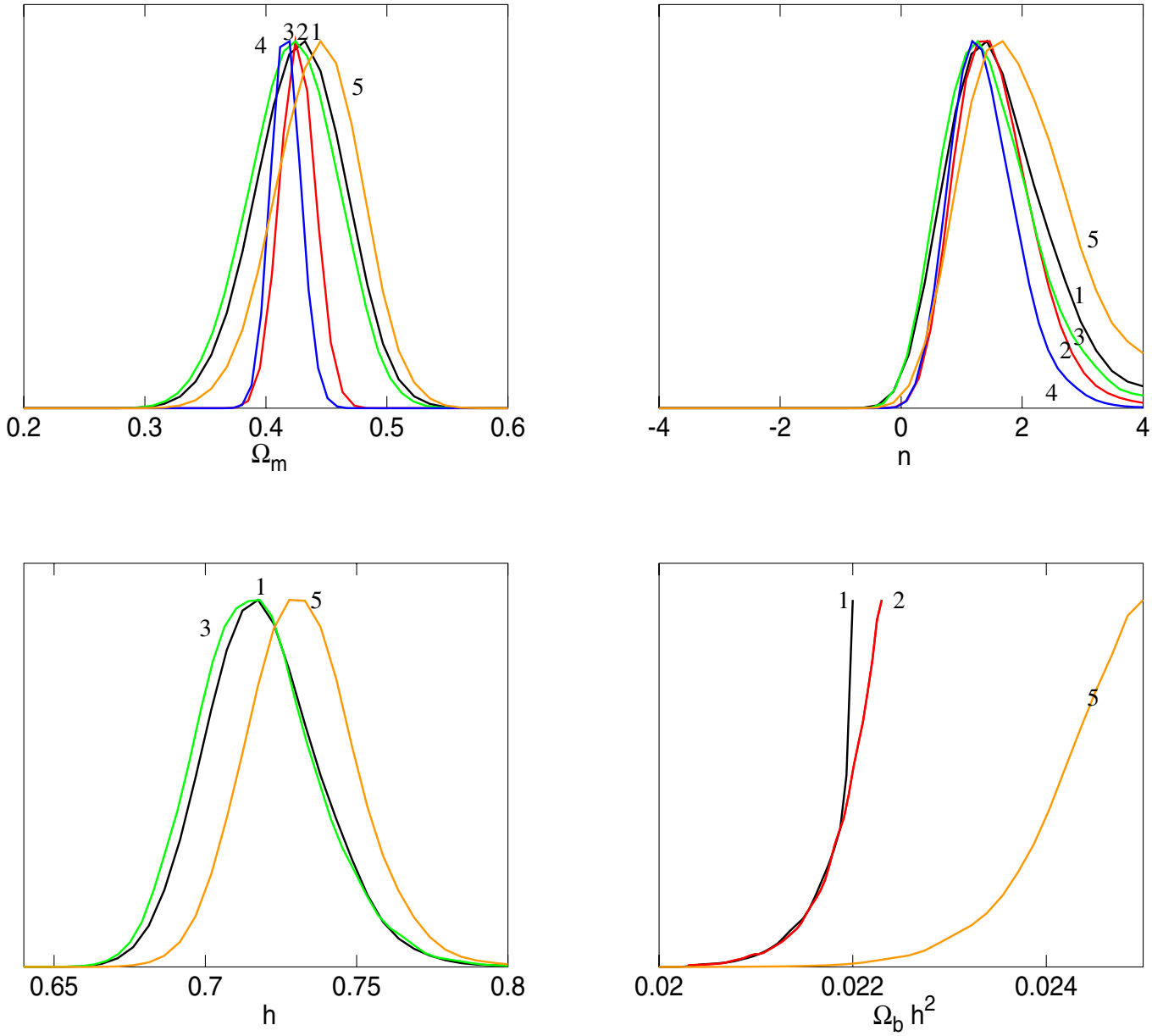

FIG. 7 (color online). Marginal posterior PDFs for model parameters (Union + CMB + BAO) with different prior assumptions on the parameters h and $\Omega_b h^2$: case 1, case 2, case 3, case 4, case 5.

to as model 0). In the Bayesian framework, models are compared not only by how well they fit the data, but also by their complexity (see [25] for a review). The best model from the set of models under consideration is the one with the greatest value of the probability in the light of data defined as

$$P(M_i|D) = \frac{P(D|M_i)P(M_i)}{P(D)}, \tag{20}$$

where M_i is a model under consideration and $P(M_i)$ is the prior probability of a model. If we have no foundation for favoring one model in the set of models under consideration over another, we usually assume the same value of the prior quantity for all models, i.e. $P(M_i) = 1/K$, where K is the number of models. $P(D)$ is the normalization constant. $P(D|M_i)$ is called the marginal likelihood (or the evidence) and has the following form:

$$P(D|M_i) = \int L(\bar{\theta})P(\bar{\theta}|M_i)d\bar{\theta} \equiv E_i. \tag{21}$$

It is convenient to consider the ratio of posterior probabilities for the models which we want to compare. If prior probabilities for those models are equal, then the posterior ratio reduces to the ratio of the evidences. This ratio is called the Bayes factor ($B_{ij} \equiv E_i/E_j$). The values of B_{ij} are interpreted as follows: $0 < \ln B_{ij} < 1$ as inconclusive,

TABLE III. Values of the logarithm of the Bayes factor $\ln B_{ij}$ calculated for the model indexed by i and the model indexed by j for different priors and different data sets.

Case	Data set	$\ln B_{01}$	$\ln B_{21}$	$\ln B_{02}$	$\ln B_{03}$	$\ln B_{31}$	$\ln B_{04}$	$\ln B_{41}$
1	SNLS	0.89 ± 0.10	-0.22 ± 0.10	1.11 ± 0.10	1.15 ± 0.07	-0.25 ± 0.07	1.06 ± 0.12	-0.17 ± 0.12
	Union	0.48 ± 0.08	-0.13 ± 0.09	0.61 ± 0.10	0.74 ± 0.09	-0.26 ± 0.08	-0.69 ± 0.09	-0.21 ± 0.08
	SNLS + CMB	5.52 ± 0.14	3.78 ± 0.27	1.74 ± 0.25	1.73 ± 0.21	3.79 ± 0.24	1.87 ± 0.31	3.65 ± 0.33
	Union + CMB	4.94 ± 0.15	3.28 ± 0.13	1.66 ± 0.15	1.59 ± 0.22	3.34 ± 0.21	1.73 ± 0.22	3.21 ± 0.21
	SNLS + CMB + BAO	4.77 ± 0.12	3.13 ± 0.19	1.64 ± 0.17	1.83 ± 0.21	2.93 ± 0.23	1.78 ± 0.16	2.99 ± 0.18
	Union + CMB + BAO	4.23 ± 0.08	2.58 ± 0.18	1.65 ± 0.17	1.66 ± 0.11	2.57 ± 0.12	1.80 ± 0.11	2.43 ± 0.12
2	SNLS + CMB	4.52 ± 0.20	3.17 ± 0.24	1.35 ± 0.16	1.50 ± 0.10	3.02 ± 0.21	1.36 ± 0.15	3.16 ± 0.23
	Union + CMB	4.40 ± 0.13	2.78 ± 0.10	1.62 ± 0.12	1.83 ± 0.16	2.57 ± 0.15	1.60 ± 0.12	2.80 ± 0.10
	SNLS + CMB + BAO	4.09 ± 0.10	2.53 ± 0.09	1.56 ± 0.09	1.73 ± 0.10	2.36 ± 0.10	1.55 ± 0.09	2.54 ± 0.09
	Union + CMB + BAO	4.08 ± 0.15	2.52 ± 0.12	1.55 ± 0.15	1.69 ± 0.14	2.38 ± 0.12	1.69 ± 0.13	2.38 ± 0.10
3	SNLS + CMB	6.41 ± 0.18	4.62 ± 0.17	1.78 ± 0.20	1.77 ± 0.27	4.64 ± 0.24	1.82 ± 0.15	4.59 ± 0.11
	Union + CMB	5.63 ± 0.19	4.13 ± 0.23	1.50 ± 0.25	1.63 ± 0.21	4.00 ± 0.19	1.67 ± 0.22	3.96 ± 0.20
	SNLS + CMB + BAO	5.67 ± 0.06	3.82 ± 0.20	1.84 ± 0.20	1.89 ± 0.11	3.77 ± 0.12	2.02 ± 0.08	3.65 ± 0.09
	Union + CMB + BAO	5.15 ± 0.17	3.47 ± 0.13	1.69 ± 0.17	1.97 ± 0.18	3.18 ± 0.14	1.90 ± 0.21	3.25 ± 0.18
4	SNLS + CMB	5.21 ± 0.12	3.99 ± 0.13	1.22 ± 0.10	1.39 ± 0.11	3.82 ± 0.13	1.20 ± 0.17	4.01 ± 0.19
	Union + CMB	4.98 ± 0.06	3.48 ± 0.12	1.50 ± 0.12	1.49 ± 0.13	3.49 ± 0.13	1.38 ± 0.22	3.59 ± 0.22
	SNLS + CMB + BAO	4.90 ± 0.09	3.41 ± 0.16	1.49 ± 0.17	1.60 ± 0.11	3.30 ± 0.09	1.62 ± 0.10	3.28 ± 0.08
	Union + CMB + BAO	4.63 ± 0.14	3.08 ± 0.15	1.55 ± 0.11	1.76 ± 0.12	2.87 ± 0.16	1.76 ± 0.18	2.88 ± 0.21
5	SNLS + CMB	2.85 ± 0.12	1.26 ± 0.27	1.59 ± 0.27	1.53 ± 0.12	1.32 ± 0.12	1.77 ± 0.14	1.08 ± 0.14
	Union + CMB	2.28 ± 0.21	0.77 ± 0.20	1.51 ± 0.17	1.38 ± 0.20	0.90 ± 0.22	1.47 ± 0.22	0.81 ± 0.24
	SNLS + CMB + BAO	1.88 ± 0.21	0.89 ± 0.22	0.99 ± 0.15	0.92 ± 0.13	0.96 ± 0.20	0.94 ± 0.14	0.93 ± 0.21
	Union + CMB + BAO	1.42 ± 0.14	0.73 ± 0.22	0.69 ± 0.20	0.58 ± 0.21	0.83 ± 0.23	0.66 ± 0.14	0.75 ± 0.17

$1 < \ln B_{ij} < 2.5$ as weak, $2.5 < \ln B_{ij} < 5$ as moderate and $\ln B_{ij} > 5$ as strong evidence in favor of a model indexed by i with respect to a model indexed by j. The evidence [Eq. (21)] was calculated using the COSMONEST code. We generated five chains for each case to obtain the uncertainty in the computed value of the evidence. We performed our calculations using the different prior assumptions for the parameters h and $\Omega_b h^2$, which were described in the previous section. The values of the logarithm of the Bayes factor calculated for the ΛCDM model (model 0) vs model 1 (i.e. the model presented in Sec. III A)—B_{01}—are presented in Table III and in Fig. 8.

The comparison in the light of the SNIa data does not give conclusive results—this data set has not enough information to favor one model over another. After the inclusion of information coming from the CMB, there is strong (SNLS + CMB) and almost strong (Union + CMB) evidence in favor of the ΛCDM model over the inhomogeneous one. When we include information coming from the BAO, the values of the Bayes factor become smaller in both cases and the evidence in favor the ΛCDM model is moderate.

Let us consider the influence of the prior information for the h and $\Omega_b h^2$ parameters on the evidence. The most prominent change is when the range of $\Omega_b h^2$ is extended (case 5). The evidence in favor of the ΛCDM model is moderate for the SNLS + CMB data set and weak otherwise. When the value of h is fixed (case 2), the value of $\ln B$ becomes smaller for all data sets and the evidence in favor of the ΛCDM model is moderate. On the other hand, fixing the value of $\Omega_b h^2$ (case 3) shifts the value of $\ln B$ upwards and the evidence in favor the ΛCDM model becomes strong. Fixing both h and $\Omega_b h^2$ (case 4) does not change the final conclusions.

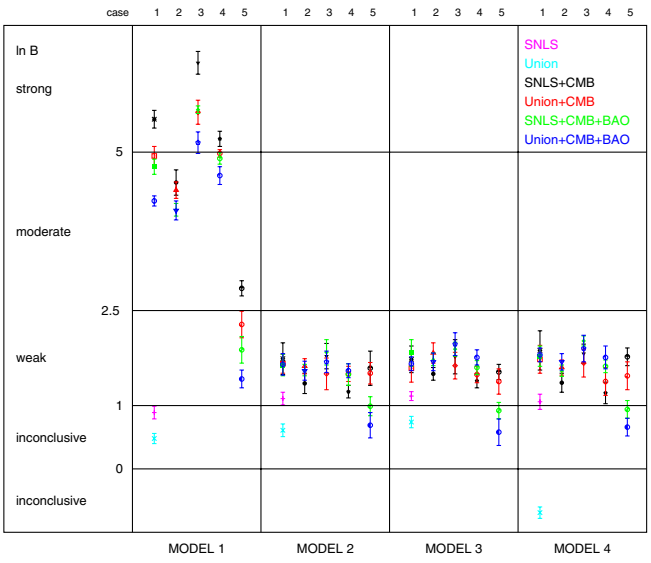

FIG. 8 (color online). Values of the logarithm of the Bayes factor $\ln B_{0i}$ calculated for the ΛCDM model and the model indexed by i for five different prior cases and different data sets (SNLS, Union, SNLS + CMB, Union + CMB, SNLS + CMB + BAO, Union + CMB + BAO).

TABLE IV. Values of the logarithm of the Bayes factor $\ln B_{01}$ calculated for the ΛCDM model and model 1 with the assumption that $n \in [-2, 3]$ for different priors and different data sets.

Data set	Case 1	Case 2	Case 3	Case 4	Case 5
SNLS	0.62 ± 0.11	...	...	...	...
Union	0.17 ± 0.14	...	...	...	...
SNLS + CMB	5.14 ± 0.16	4.12 ± 0.13	5.84 ± 0.18	4.79 ± 0.10	2.36 ± 0.13
Union + CMB	4.48 ± 0.17	4.00 ± 0.14	5.13 ± 0.17	4.53 ± 0.15	1.86 ± 0.18
SNLS + CMB + BAO	4.32 ± 0.15	3.81 ± 0.14	5.32 ± 0.05	4.49 ± 0.18	1.72 ± 0.14
Union + CMB + BAO	3.80 ± 0.11	3.56 ± 0.19	4.61 ± 0.19	4.32 ± 0.12	1.19 ± 0.18

It is also interesting to see how strong is the influence of the prior information regarding the n parameter on the final results. We repeat our calculations for the case in which the prior range for the n parameter is changed, i.e. for $n \in [-2, 3]$. The values of the logarithm of the Bayes factor calculated with respect to the ΛCDM model for different data sets and different prior cases regarding the h and $\Omega_b h^2$ parameters are presented in Table IV and in Fig. 9.

Observe that, when the prior range for n is restricted, the values of the logarithm of the Bayes factor become smaller, but the differences in the case in which $n \in [-4, 4]$ are small. Considering the comparison with the ΛCDM model, one finds that in general the final conclusions do not change.

2. Relation between the average curvature and the curvature index

In the preceding subsection we could see that the Bayesian method of model comparison prefers the ΛCDM model over the backreaction model. We should be aware that the backreaction model—model 1—is based on the assumptions (9) and (10). If these assumptions are changed, it is possible to obtain a model with a better fit.

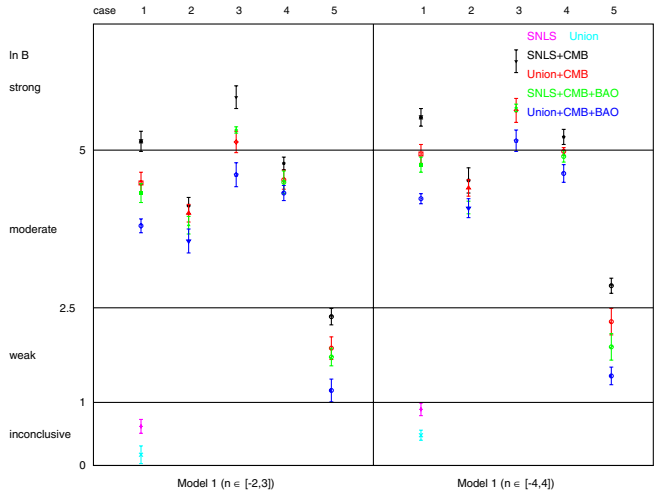

FIG. 9 (color online). Values of logarithm of the Bayes factor $\ln B_{01}$ calculated for the ΛCDM model and model 1 (with two different prior assumptions on n parameter) for five different prior cases (regarding h and $\Omega_b h^2$ parameters) and different data sets (SNLS, Union, SNLS + CMB, Union + CMB, SNLS + CMB + BAO, Union + CMB + BAO).

Below we present models in which the assumption (10) is replaced with

(i) model 2

$$k(z) = 0. \tag{22}$$

We emphasize that $k = 0$ comes from a modification of the assumption (10) only. It is not the same as assuming that $\langle \mathcal{R} \rangle = 0$. As seen from (5) the assumption of $\langle \mathcal{R} \rangle = 0$ leads to $\mathcal{Q} \sim a^{-6}$, which means that the backreaction is strong in the early Universe and its value decreases with time.

The results of the model comparison are presented in Table III and in Fig. 8. As can be seen, both for the SNIa + CMB and SNIa + CMB + BAO data sets, there is moderate evidence to favor the backreaction model with $k = 0$ over the model with relation (10). Note that there is only weak evidence to favor the ΛCDM model over model 2. A change in the prior information regarding h and $\Omega_b h^2$ does not change the final conclusions for all considered cases, besides case 5. When the range for the parameter $\Omega_b h^2$ is extended, the evidence against model 1 becomes smaller.

(ii) model 3

$$k(z) = -\frac{1}{p}(1+z)^{-(n+2)}. \tag{23}$$

We assume a flat prior PDF for the additional parameter in the range $p \in [0, 100]$. Observe that, model 2 fits the observations better than model 1. If indeed $k = 0$ is favored, then we should obtain that the best model with k given by (23) is the one with $p = 100$. However, this is not the case and as seen from Fig. 10, the marginal posterior PDF is almost flat over a very wide range—there is only a little difference between $p = 100$ and the best-fit value. This conclusion is confirmed bu observing the value of the logarithm of the Bayes factor: there

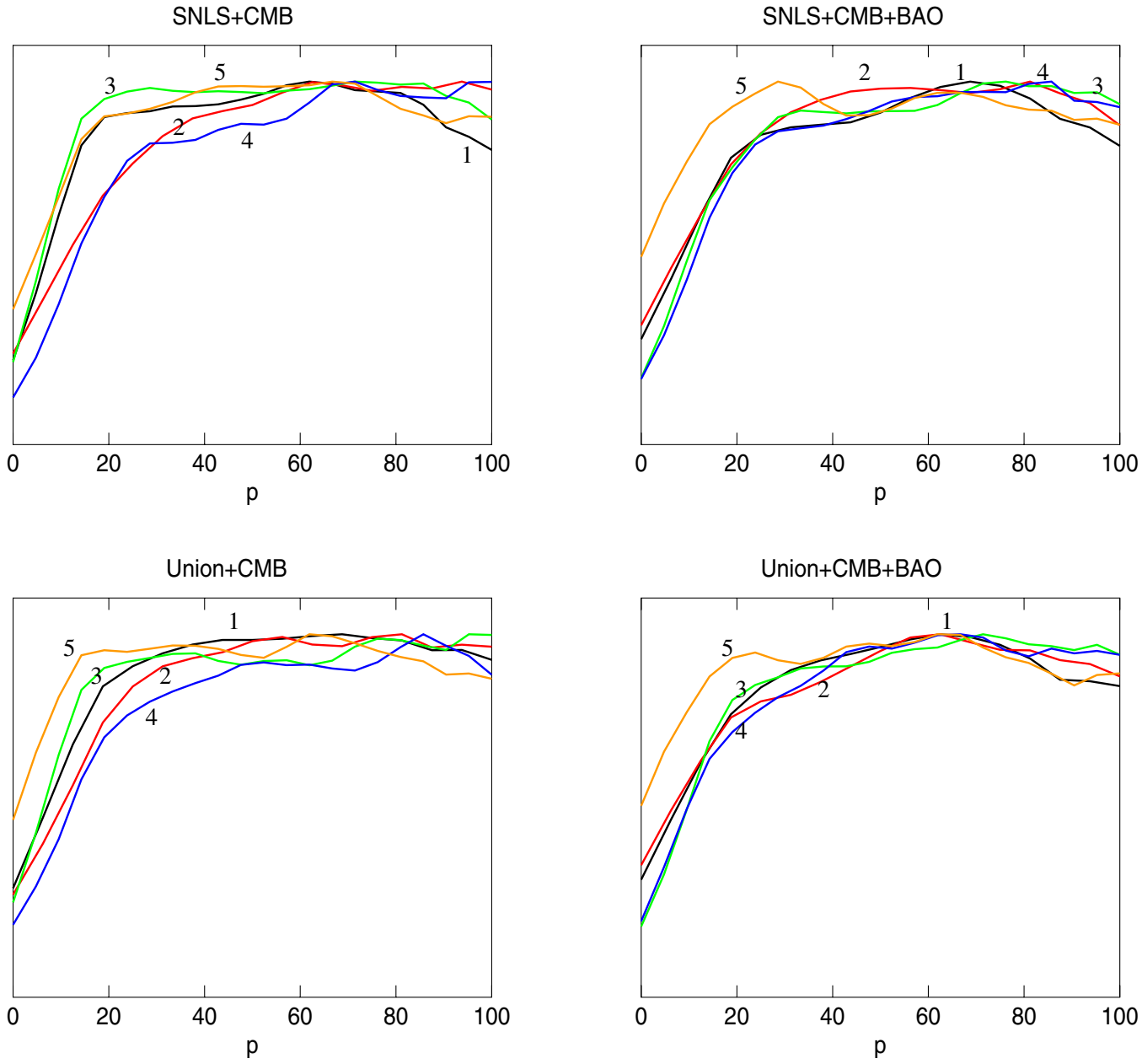

FIG. 10 (color online). Marginal posterior PDF for the parameter p of model 3 with different prior assumptions on the h and $\Omega_b h^2$ parameters: case 1, case 2, case 3, case 4, case 5.

is not enough information to favor model 2 over model 3. The means and modes of the marginal posterior PDFs for the model parameters are presented in Table V. The values of the logarithm of the Bayes factor, calculated for the ΛCDM model and model 3 ($\ln B_{03}$), as well as for model 3 and model 1 ($\ln B_{31}$) are compared in Table III (see also Fig. 8). One may conclude that there is weak evidence to favor the ΛCDM model over model 3 and moderate evidence in favor of model 3 over model 1 (for the SNIa + CMB and SNIa + CMB + BAO data sets). The conclusion is changed when the range for $\Omega_b h^2$ is extended: for the SNIa + CMB + BAO data set, the evidence in favor of the ΛCMD model becomes inconclusive.

(iii) model 4

$$k(z) = -(1+z)^{-(n+2+m)}. \tag{24}$$

We assume a flat prior PDF for the additional parameter in the range $m \in [0, 5]$. The marginal posterior PDF for the parameter m is presented in Fig. 11. The means and modes of the marginal

TABLE V. Mean of the marginal posterior PDF for the parameters of model 3, together with the 68% credible interval, for the SNIa + CMB and SNIa + CMB + BAO data sets. The corresponding values of posterior mode are presented in brackets.

	SNLS + CMB	SNLS + CMB + BAO	Union + CMB	Union + CMB + BAO
Ω_m	$0.24^{+0.04}_{-0.03}(0.20)$	$0.28^{+0.06}_{-0.05}(0.27)$	$0.26^{+0.05}_{-0.05}(0.20)$	$0.31^{+0.06}_{-0.07}(0.31)$
n	$-0.18^{+0.28}_{-0.33}(-0.37)$	$0.10^{+0.54}_{-0.55}(-0.20)$	$-0.13^{+0.37}_{-0.41}(-0.53)$	$0.27^{+0.70}_{-0.67}(0.16)$
h	$0.76^{+0.02}_{-0.02}(0.78)$	$0.74^{+0.02}_{-0.02}(0.74)$	$0.75^{+0.02}_{-0.02}(0.77)$	$0.73^{+0.02}_{-0.02}(0.73)$
$\Omega_b h^2$	$0.0216^{+0.0005}_{-0.0005}(0.0222)$	$0.0216^{+0.0005}_{-0.0006}(0.0221)$	$0.0216^{+0.0005}_{-0.0006}(0.0221)$	$0.0217^{+0.0005}_{-0.0006}(0.0223)$
p	$53.18^{+30.63}_{-31.26}(75.80)$	$54.25^{+30.09}_{-31.01}(63.71)$	$53.99^{+30.97}_{-31.19}(50.23)$	$53.87^{+30.26}_{-30.43}(48.61)$
Ω_m	$0.30^{+0.06}_{-0.05}(0.28)$	$0.32^{+0.06}_{-0.05}(0.32)$	$0.32^{+0.05}_{-0.05}(0.34)$	$0.33^{+0.05}_{-0.05}(0.34)$
n	$-0.01^{+0.64}_{-0.63}(-0.35)$	$0.30^{+0.81}_{-0.77}(-0.01)$	$0.18^{+0.66}_{-0.66}(0.30)$	$0.44^{+0.76}_{-0.77}(0.31)$
h	0.72	0.72	0.72	0.72
$\Omega_b h^2$	$0.0216^{+0.0005}_{-0.0007}(0.0220)$	$0.0216^{+0.0006}_{-0.0006}(0.0222)$	$0.0216^{+0.0006}_{-0.0005}(0.0223)$	$0.0217^{+0.0005}_{-0.0005}(0.0223)$
p	$56.14^{+30.28}_{-30.46}(87.19)$	$54.35^{+30.59}_{-30.26}(61.34)$	$55.19^{+30.44}_{-30.54}(73.54)$	$54.29^{+30.89}_{-31.33}(73.01)$
Ω_m	$0.24^{+0.03}_{-0.03}(0.20)$	$0.27^{+0.05}_{-0.05}(0.23)$	$0.25^{+0.04}_{-0.04}(0.20)$	$0.29^{+0.06}_{-0.06}(0.24)$
n	$-0.24^{+0.28}_{-0.30}(-0.48)$	$-0.04^{+0.46}_{-0.47}(-0.31)$	$-0.23^{+0.31}_{-0.34}(-0.57)$	$0.08^{+0.59}_{-0.57}(-0.33)$
h	$0.76^{+0.02}_{-0.02}(0.77)$	$0.74^{+0.03}_{-0.02}(0.76)$	$0.75^{+0.02}_{-0.02}(0.76)$	$0.73^{+0.02}_{-0.02}(0.75)$
$\Omega_b h^2$	0.0213	0.0213	0.0213	0.0213
p	$53.09^{+31.72}_{-31.59}(89.47)$	$55.33^{+30.73}_{-30.56}(61.07)$	$53.62^{+31.94}_{-32.17}(32.14)$	$55.03^{+30.79}_{-31.23}(84.36)$
Ω_m	$0.29^{+0.04}_{-0.05}(0.26)$	$0.31^{+0.05}_{-0.05}(0.26)$	$0.30^{+0.05}_{-0.04}(0.27)$	$0.32^{+0.04}_{-0.05}(0.28)$
n	$-0.19^{+0.52}_{-0.51}(-0.57)$	$0.01^{+0.72}_{-0.57}(-0.54)$	$-0.02^{+0.56}_{-0.56}(-0.42)$	$0.20^{+0.63}_{-0.63}(-0.31)$
h	0.72	0.72	0.72	0.72
$\Omega_b h^2$	0.0213	0.0213	0.0213	0.0213
p	$56.95^{+29.88}_{-30.45}(76.57)$	$55.75^{+29.97}_{-30.44}(78.65)$	$55.84^{+30.50}_{-30.70}(91.07)$	$55.37^{+30.50}_{-30.49}(96.67)$
Ω_m	$0.31^{+0.07}_{-0.07}(0.26)$	$0.37^{+0.07}_{-0.07}(0.36)$	$0.34^{+0.07}_{-0.07}(0.32)$	$0.38^{+0.06}_{-0.05}(0.41)$
n	$0.48^{+0.80}_{-0.75}(0.00)$	$1.28^{+1.16}_{-1.10}(1.14)$	$0.73^{+0.87}_{-0.86}(0.42)$	$1.32^{+0.97}_{-0.96}(1.57)$
h	$0.76^{+0.02}_{-0.03}(0.78)$	$0.74^{+0.02}_{-0.02}(0.75)$	$0.74^{+0.03}_{-0.03}(0.76)$	$0.73^{+0.02}_{-0.02}(0.73)$
$(\Omega_b h^2)^*$	$0.0238^{+0.0010}_{-0.0009}(0.0248)$	$0.0240^{+0.0008}_{-0.0008}(0.0249)$	$0.0240^{+0.0008}_{-0.0007}(0.0249)$	$0.0241^{+0.0007}_{-0.0007}(0.0248)$
p	$52.61^{+31.47}_{-31.78}(34.64)$	$51.43^{+32.48}_{-32.23}(76.04)$	$51.34^{+32.46}_{-32.52}(37.58)$	$51.44^{+32.02}_{-32.32}(22.30)$

posterior PDF for the model parameters are presented in Table VI. The values of logarithm of the Bayes factor calculated for the ΛCDM model and model 4 ($\ln B_{04}$) as well as for model 4 and model 1 ($\ln B_{41}$) are compared in Table III (see also Fig. 8). Observe that there is weak evidence to favor the ΛCDM model over model 4 for the all considered cases, besides case 5 and for the SNIa + CMB + BAO data sets, where the comparison is inconclusive. The differences in the values of the evidence between model 4 and model 2 or model 3 are small, which leads to the conclusion that there is insufficient information to favor the former. Model 4 is better than model 1 in light of the data used in this analysis, with moderate evidence against the latter. This conclusion is changed in case 5, in which the value of the Bayes factor calculated for those models becomes smaller.

Observe that except for the SNLS + CMB a change in the priors for h and $\Omega_b h^2$ does not change the shape of the posterior PDF for m, which is flat for $m > 3$. For the SNLS + CMB data, the posterior is wider, it is flat for $m > 2$ and becomes narrower when the value of h is fixed. When the range of $\Omega_b h^2$ is extended, the posterior PDF for m becomes wider in all cases.

The above results are encouraging and motivate further study of the backreaction models. Especially, it is important to study assumptions other than (9) and (10). As seen, if only assumption (10) was modified (models 2–4) then not only do we obtained a better fit, but also the value of Ω_m realistically decreases compared to model 1.

IV. CONCLUSIONS

In this paper we presented a Bayesian analysis of the backreaction models. This work was motivated by the recently proposed model of the inhomogeneous alternative to dark energy [8]. In this approach the Universe is modeled by the Buchert equations, which describe the relations between the scale factor, the average spatial curvature, the average matter distribution, the average expansion and the shear. Larena *et al.* [8] showed that their model is consistent with supernova and CMB data. Here, we included the BAO data and tested this model within the Bayesian approach (our model 1).

Our analysis shows that the SNLS and CMB data alone strongly favor the ΛCDM model. With the Union sample

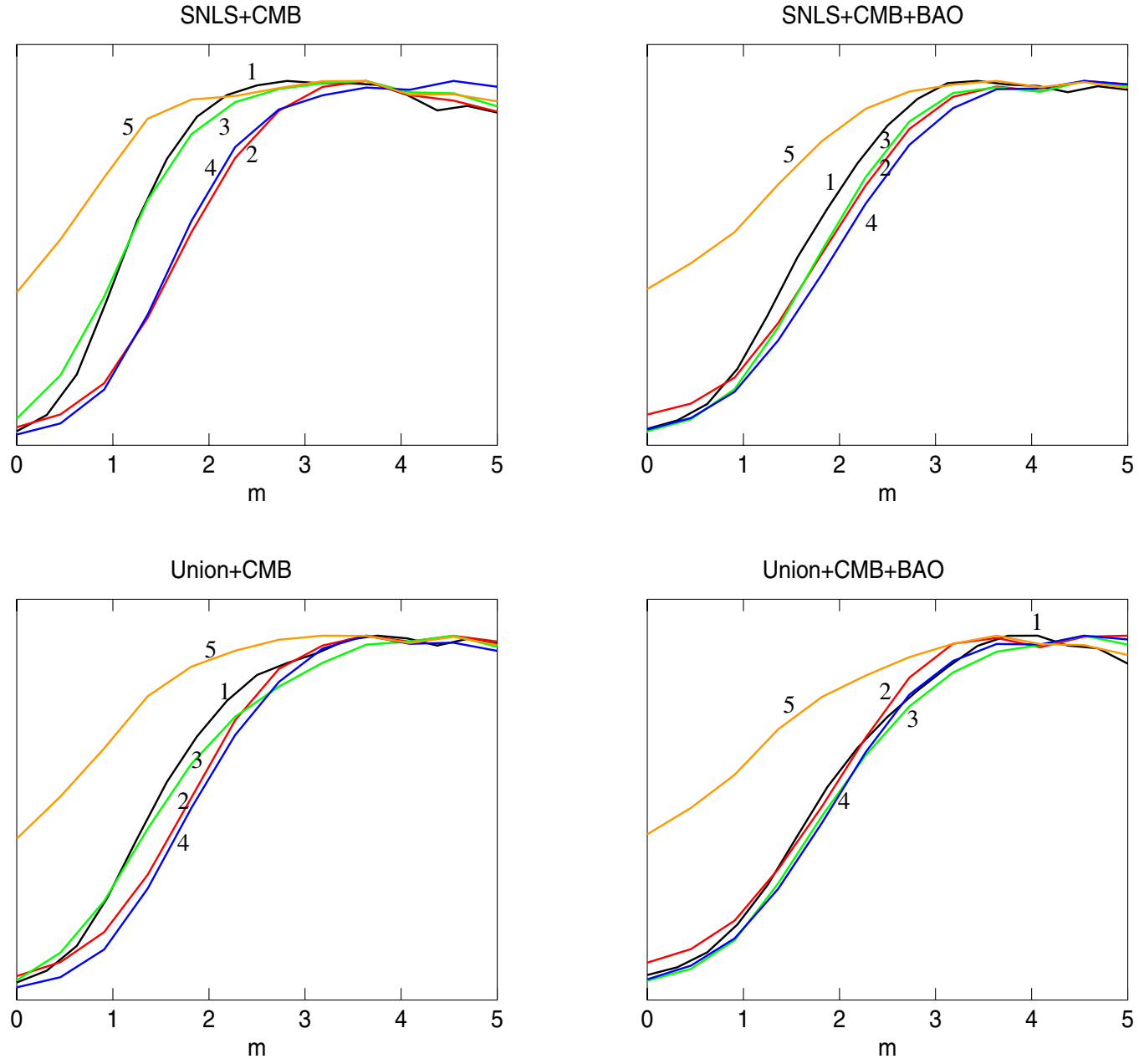

FIG. 11 (color online). Marginal posterior PDF for the parameter m of model 4 with different prior assumptions on the h and $\Omega_b h^2$ parameters: case 1, case 2, case 3, case 4, case 5.

and BAO data there is almost strong evidence ($\ln B_{21} > 4$) to favor the ΛCDM model over our model 1. However, if just the best-fit models are compared, then the χ^2 (Union + CMB + BAO) for the ΛCDM and model 1 are 320.96 and 325.36, respectively. If the χ^2 distribution is assumed, then for 307 degrees of freedom in model 1 the probability that this model is true in the light of data is 22.6%. In comparison, the ΛCDM model (308 degrees of freedom) gives 29.3%. Therefore, we can see that the best-fit model 1 fits observations almost as well as the ΛCDM model. Still, there are other concerns regarding this model. For example, can the assumptions (9) and (10) be justified? In other words, how does the backreaction and the spatial curvature of the real Universe evolve, and does the relation $\mathcal{Q} \sim \langle \mathcal{R} \rangle$ for the real Universe hold? The most concerning is the value of Ω_m, which is quite large, $0.43^{+0.03}_{-0.04}$. However, as it was shown in Sec. III B 2, after the assumption (10) was modified, we were able to obtain a better fit and, in addition, the value of Ω_m decreased to $0.31^{+0.06}_{-0.07}$ and $0.30^{+0.07}_{-0.06}$ (or even lower if the BAO data is excluded—see Tables V and VI) for models 4 and 5, respectively. This shows that a lot still needs to be done in the context of

TABLE VI. Mean of the marginal posterior PDF for the parameters of model 4, together with the 68% credible interval, for the SNIa + CMB and SNIa + CMB + BAO data sets. The corresponding values of posterior mode are presented in brackets.

	SNLS + CMB	SNLS + CMB + BAO	Union + CMB	Union + CMB + BAO
Ω_m	$0.24^{+0.04}_{-0.03}(0.20)$	$0.28^{+0.06}_{-0.06}(0.25)$	$0.26^{+0.05}_{-0.05}(0.23)$	$0.30^{+0.07}_{-0.06}(0.26)$
n	$-0.32^{+0.29}_{-0.34}(-0.58)$	$-0.06^{+0.52}_{-0.54}(-0.37)$	$-0.26^{+0.40}_{-0.40}(-0.56)$	$0.07^{+0.69}_{-0.65}(-0.38)$
h	$0.76^{+0.02}_{-0.03}(0.77)$	$0.74^{+0.02}_{-0.02}(0.75)$	$0.74^{+0.02}_{-0.02}(0.75)$	$0.73^{+0.02}_{-0.02}(0.74)$
$\Omega_b h^2$	$0.0216^{+0.0005}_{-0.0006}(0.0220)$	$0.0216^{+0.0005}_{-0.0006}(0.0221)$	$0.0216^{+0.0005}_{-0.0006}(0.0222)$	$0.0216^{+0.0005}_{-0.0006}(0.0220)$
m	$3.00^{+1.34}_{-1.31}(3.05)$	$3.20^{+1.23}_{-1.22}(3.18)$	$3.13^{+1.29}_{-1.28}(3.79)$	$3.22^{+1.22}_{-1.24}(3.61)$
Ω_m	$0.29^{+0.06}_{-0.05}(0.25)$	$0.31^{+0.06}_{-0.06}(0.29)$	$0.30^{+0.06}_{-0.05}(0.30)$	$0.32^{+0.06}_{-0.06}(0.31)$
n	$-0.24^{+0.58}_{-0.57}(-0.64)$	$0.04^{+0.79}_{-0.73}(-0.33)$	$-0.10^{+0.65}_{-0.62}(-0.24)$	$0.17^{+0.78}_{-0.74}(-0.15)$
h	0.72	0.72	0.72	0.72
$\Omega_b h^2$	$0.0215^{+0.0006}_{-0.0006}(0.0219)$	$0.0216^{+0.0005}_{-0.0007}(0.0222)$	$0.0216^{+0.0005}_{-0.0007}(0.0222)$	$0.0217^{+0.0005}_{-0.0006}(0.0222)$
m	$3.23^{+1.18}_{-1.16}(4.21)$	$3.25^{+1.23}_{-1.19}(4.79)$	$3.25^{+1.20}_{-1.16}(4.83)$	$3.22^{+1.25}_{-1.19}(3.55)$
Ω_m	$0.24^{+0.03}_{-0.03}(0.20)$	$0.26^{+0.05}_{-0.04}(0.22)$	$0.25^{+0.04}_{-0.04}(0.21)$	$0.28^{+0.07}_{-0.05}(0.22)$
n	$-0.38^{+0.26}_{-0.30}(-0.55)$	$-0.23^{+0.39}_{-0.43}(-0.50)$	$-0.36^{+0.33}_{-0.35}(-0.64)$	$-0.11^{+0.54}_{-0.55}(-0.66)$
h	$0.76^{+0.02}_{-0.03}(0.76)$	$0.74^{+0.02}_{-0.02}(0.75)$	$0.74^{+0.02}_{-0.02}(0.75)$	$0.73^{+0.02}_{-0.02}(0.74)$
$\Omega_b h^2$	0.0213	0.0213	0.0213	0.0213
m	$3.00^{+1.34}_{-1.33}(4.69)$	$3.29^{+1.19}_{-1.15}(4.50)$	$3.17^{+1.26}_{-1.28}(4.15)$	$3.30^{+1.18}_{-1.19}(3.93)$
Ω_m	$0.28^{+0.04}_{-0.05}(0.24)$	$0.29^{+0.06}_{-0.05}(0.24)$	$0.29^{+0.05}_{-0.05}(0.25)$	$0.30^{+0.06}_{-0.05}(0.26)$
n	$-0.39^{+0.44}_{-0.47}(-0.76)$	$-0.16^{+0.62}_{-0.58}(-0.73)$	$-0.27^{+0.52}_{-0.50}(-0.64)$	$-0.05^{+0.62}_{-0.60}(-0.52)$
h	0.72	0.72	0.72	0.72
$\Omega_b h^2$	0.0213	0.0213	0.0213	0.0213
m	$3.26^{+1.20}_{-1.17}(3.23)$	$3.33^{+1.16}_{-1.14}(3.66)$	$3.30^{+1.16}_{-1.14}(3.87)$	$3.30^{+1.19}_{-1.16}(4.33)$
Ω_m	$0.31^{+0.08}_{-0.07}(0.25)$	$0.38^{+0.07}_{-0.08}(0.35)$	$0.34^{+0.08}_{-0.07}(0.34)$	$0.39^{+0.06}_{-0.06}(0.40)$
n	$0.37^{+0.83}_{-0.79}(-0.22)$	$1.19^{+1.21}_{-1.16}(0.70)$	$0.60^{+0.86}_{-0.85}(0.47)$	$1.25^{+1.01}_{-0.99}(1.43)$
h	$0.76^{+0.02}_{-0.03}(0.77)$	$0.74^{+0.02}_{-0.03}(0.75)$	$0.74^{+0.02}_{-0.02}(0.75)$	$0.73^{+0.02}_{-0.02}(0.74)$
$(\Omega_b h^2)^*$	$0.0239^{+0.0009}_{-0.0010}(0.0248)$	$0.0240^{+0.0008}_{-0.0008}(0.0248)$	$0.0241^{+0.0007}_{-0.0008}(0.0249)$	$0.0241^{+0.0007}_{-0.0007}(0.0249)$
m	$2.72^{+1.54}_{-1.52}(3.32)$	$2.82^{+1.49}_{-1.52}(4.10)$	$2.75^{+1.54}_{-1.54}(3.55)$	$2.79^{+1.51}_{-1.56}(3.23)$

the backreaction models, especially in the study of the relation between the average spatial curvature and the backreaction.

We also investigated the sensitivity of the results to the prior assumptions on the h, $\Omega_b h^2$ and n parameters. The most prominent changes are in the case in which the Hubble parameter is fixed and in the case in which the range of the parameter $\Omega_b h^2$ is extended. In the latter case, the evidence against model 1 with respect to the ΛCDM model is weak.

Currently, the ΛCDM model is preferred by the observational data, but it is possible that, after the revision of assumptions (9) and (10) we could obtain a more satisfactory results (see Table III and Fig. 8). We should also remember that in these models of dark energy, the dark-energy-term appears as a consequence of inhomogeneities that are present in the Universe. Therefore, within this class of models, the ''decaying lambda term'' takes on reveals a new and natural interpretation.

ACKNOWLEDGMENTS

This research was supported by the Marie Curie COCOS project under Contract No. MTKD-CT-2004-517186 (A. K., M. S.) and partly by the Peter and Patricia Gruber Foundation and the International Astronomical Union (K. B.). M. S. is very grateful to M. Carfora for discussions and the warm atmosphere during the visit in Pavia. We also thank A. Prinsloo for helpful comments.

[1] K. Koyama, Gen. Relativ. Gravit. **40**, 421 (2008).
[2] S. Capozziello and M. Francaviglia, Gen. Relativ. Gravit. **40**, 357 (2008).
[3] M. N. Célérier, New Adv. Phys. **1**, 29 (2007).
[4] T. Buchert, Gen. Relativ. Gravit. **32**, 105 (2000).
[5] S. Räsänen, J. Cosmol. Astropart. Phys. 11 (2006) 003.
[6] T. Buchert, Gen. Relativ. Gravit. **40**, 467 (2008).
[7] T. Buchert and M. Carfora, Classical Quantum Gravity **25**,

195001 (2008).
[8] J. Larena, J.-M. Alimi, T. Buchert, M. Kunz, and P.-S. Corasaniti, Phys. Rev. D **79**, 083011 (2009).
[9] A. Paranjape and T. P. Singh, Gen. Relativ. Gravit. **40**, 139 (2008).
[10] G. F. R. Ellis and W. Stoeger, Classical Quantum Gravity **4**, 1697 (1987).
[11] P. Mukherjee, D. Parkinson, and A. R. Liddle, Astrophys. J. Lett. **51**, 638 (2006); code available from http://www.cosmonest.org/.
[12] The COSMONEST code uses the nested sampling algorithm [13] and is a part of the COSMOMC code [14].
[13] J. Skilling, *Bayesian Inference and Maximum Entropy Methods in Science and Engineering*, AIP Conf. Proc. No. 735 (AIP, New York, 2004), p 395; http://www.inference.phy.cam.ac.uk/bayesys/.
[14] A. Lewis and S. Bridle, Phys. Rev. D **66**, 103511 (2002); code available from http://cosmologist.info/cosmomc/.
[15] P. Astier *et al.*, Astron. Astrophys. **447**, 31 (2006).
[16] M. Kowalski *et al.*, Astrophys. J. **686**, 749 (2008).
[17] SNLS error estimation includes: photometric uncertainty, uncertainty due to host galaxy peculiar velocities of 300 km/s, uncertainty of 0.13104 mag related to intrinsic dispersion of SNe Ia. UNION statistical uncertainty was obtained from the light-curve fit.
[18] The distance estimator was assumed to be $\mu^{\rm obs} = m_B - M + \alpha(s-1) - \beta c$. Where m_B (supernova B-band maximum magnitude), s (stretch), and c (color) were derived from the fit to the light curves. We took the observational data at face value without correcting it for such effects as gravitational lensing.
[19] M. Doran and M. Lilley, Mon. Not. R. Astron. Soc. **330**, 965 (2002).
[20] We justify this approach by emphasizing that backreaction effects are still not fully understood, and there is an ongoing debate on how large is the amplitude of these effects. Analysis of the position of the CMB peaks is straightforward, and it quickly allows to test if models are consistent with the data. Once the backreactions effects are better understood a full analysis will be required.
[21] G. Hinshaw *et al.*, Astrophys. J. Suppl. Ser. **170**, 288 (2007).
[22] W. Hu and N. Sugiyama, Astrophys. J. **471**, 542 (1996).
[23] W. L. Freedman *et al.*, Astrophys. J. **553**, 47 (2001).
[24] M. Pettini *et al.*, arXiv:0805.0594.
[25] R. Trotta, Contemp. Phys. **49**, 71 (2008).
[26] H. Jeffreys, *Theory of Probability* (Oxford University Press, Oxford, 1961).